

Charged Higgs Boson Production in Bottom-Gluon Fusion

Tilman Plehn

*Physics Department, University of Wisconsin, Madison, WI 53706, USA***Abstract**

We compute the complete next-to-leading order SUSY-QCD corrections for the associated production of a charged Higgs boson with a top quark via bottom-gluon fusion. We investigate the applicability of the bottom parton description in detail. The higher order corrections can be split into real and virtual corrections for a general two Higgs doublet model and into additional massive supersymmetric loop contributions. We find that the perturbative behavior is well under control. The supersymmetric contributions consist of the universal bottom Yukawa coupling corrections and non-factorizable diagrams. Over most of the relevant supersymmetric parameter space the Yukawa coupling corrections are sizeable, while the remaining supersymmetric loop contributions are negligible.

I. HIGGS PHYSICS AT THE LHC

In the near future the CERN Large Hadron Collider (LHC) will be the appropriate tool to look for physics beyond the Standard Model and to determine its properties. The capabilities of the LHC beyond being a pure discovery machine become increasingly important at energy scales which are hard to access at a Linear Collider.

The combined LEP precision measurements [1] suggest the existence of a light Higgs boson. In the case of a single Standard Model Higgs boson the LHC promises multiple coverage for any Higgs boson mass, which will enable us to measure its different decay modes and extract the couplings [2–4]. In the case of a supersymmetric Higgs sector this coverage becomes less impressive. This is a direct consequence of the structure of the Higgs sector: while the Minimal Supersymmetric Standard Model (MSSM) predicts a light Higgs boson it also predicts an enhancement of the coupling to down-type fermions, at the expense of the branching fractions to gauge bosons. This enhancement is an outcome from the two Higgs doublet structure in the MSSM: one doublet is needed to give mass to the up-type, the other one to the down-type fermions. The vacuum expectation values of the two doublets are different, parameterized by $\tan\beta = v_2/v_1$. The Yukawa coupling to the down-type fermions is essentially enhanced by $\tan\beta$, while the coupling to up-type fermions is suppressed by the same factor. In addition to a light scalar Higgs boson the two Higgs doublet model includes a heavy scalar, a pseudoscalar, and a charged Higgs boson. None of these additional particles have a mass bounded from above, apart from triviality or unitarity bounds. On the contrary, for a large pseudoscalar mass these three additional particles all become heavy and almost mass degenerate.

As in the Standard Model case the light scalar Higgs supersymmetric boson will be produced via gluon fusion or weak boson fusion, but it will most prominently decay to bottom quarks and tau leptons. A search for the tau lepton decay essentially covers the MSSM parameter space with a luminosity of $\sim 40 \text{ fb}^{-1}$ at the LHC [3]. The same process can be used to determine if the light Higgs boson is the scalar or the pseudoscalar mode in the two Higgs doublet model and what kind of operator governs its coupling to gauge bosons [5]. More exotic scenarios might for example lead to an invisibly decaying light Higgs boson, which again can be extracted from the backgrounds [6].

All these observables linked to properties of a light Higgs boson can serve as a probe if a new scalar particle is consistent with the Standard Model Higgs boson. There is, however, only one way to conclusively tell the supersymmetric Higgs sector from its Standard Model counterpart: to discover the additional heavy Higgs bosons and determine their properties. This task might entirely be left to the LHC, since at a Linear Collider the promising production channels are pair production of these heavy bosons, for which a first generation collider might well have insufficient energy [7]. At the LHC the possible enhancement of down-type fermion Yukawa couplings renders the search for a heavy scalar and pseudoscalar Higgs boson decaying to muon and tau lepton pairs most promising [8]. For the charged Higgs boson the coupling to fermions is more complex: for small values of $\tan\beta$ it is governed by the up-type coupling $m_u/\tan\beta$, whereas for larger values of $\tan\beta$ the down type Yukawa coupling $m_d\tan\beta$ dominates. In particular for values $\tan\beta \gtrsim 30$ the charged Higgs coupling behaves the same way as the heavy neutral Yukawa couplings. While the chances of finding a heavy Higgs boson with a small value of $\tan\beta$ at the LHC are rather slim, the discovery of all heavy Higgs scalars in the large $\tan\beta$ regime is likely.

Three search modes for the charged Higgs boson have been explored in some detail: (1) Charged Higgs bosons can be pair produced in a Drell–Yan type process, mediated by a weak interaction vertex [9]. Moreover, they can be pair produced at tree level in bottom quark scattering [10] or through a one loop amplitude in gluon fusion [11]. (2) A charged Higgs boson can be produced together with a W boson via scattering of two bottom quarks or in gluon fusion [12]. (3) The charged Higgs boson can be produced in association with a top quark, which seems to be the most promising search channel [13–15]. The charged Higgs boson can be detected either decaying to a top and a bottom quark [16] or decaying to a tau lepton and a neutrino [17]. The completely exclusive process reads ¹:

$$gg \rightarrow \bar{b}tH^- + c.c. \quad H^- \rightarrow \tau\bar{\nu}_\tau \quad \text{or} \quad H^- \rightarrow b\bar{t} \quad (1)$$

As we will argue in Section II this process can and should be evaluated in the bottom parton approximation $bg \rightarrow tH^-$, unless the observation of the additional bottom jet is necessary to extract the signal out of the background. Recently both LHC experiments have published detailed studies of this production channel with very promising results [18,19]. However, the crucial ingredient to searches and in particular to the precise extraction of couplings and masses at the LHC are next-to-leading order predictions for the signal and background cross sections. Without these improved cross section calculations theoretical uncertainties will almost immediately become the limiting factor in many analyses. The next-to-leading order cross section

¹There is an additional contribution from $q\bar{q}$ scattering, where the charged Higgs boson is produced through intermediate $b\bar{b}$ or $t\bar{t}$ states. Numerically this contribution is negligible at the LHC. It is also irrelevant for the following discussion, where we are interested in incoming gluons splitting into two bottom quarks. Therefore we omit this process in our discussion of exclusive $\bar{b}tH^-$ production at the LHC.

predictions for the inclusive production process $bg \rightarrow tH^-$ will be presented in Section III for a general two Higgs doublet model and in Section IV for the MSSM.

Conventions: Throughout this entire paper we show consistent leading order or next-to-leading order cross section predictions, including the respective one loop or two loop strong coupling constant, running heavy quark masses, and the corresponding CTEQ5L or CTEQ5M1 parton densities [20]. The bottom pole mass is fixed as 4.6 GeV, to give the correct $\overline{\text{MS}}$ mass $m_b(m_b) = 4.2$ GeV [21]. We usually assume three charged Higgs masses of 250, 500, 1000 GeV, and if not stated otherwise $\tan\beta = 30$. The exclusive cross sections are quoted with a massive (4.6 GeV) bottom quark in the matrix element and the phase space, the inclusive results are evaluated for a vanishing bottom mass. The bottom Yukawa coupling is set to the running bottom mass, unless explicitly stated as being the pole mass. When we talk about the running bottom Yukawa coupling we implicitly include the running top Yukawa coupling to the charged Higgs boson as well ($y_{b,t}(\mu_R)$), but the running of the bottom mass is the dominant effect, by far. As the central value all scales are set to the average final state mass $\mu = m_{av} = (m_t + m_H)/2$. The extension of this calculation to charged Higgs boson masses below the top mass is straightforward: to avoid double counting of diagrams which also appear in top pair production with a subsequent decay into a charged Higgs boson and a bottom jet we will have to subtract on-shell top states. This is the standard procedure for supersymmetric production processes and can be applied to light charged Higgs boson production without any modification [22,23].

II. BOTTOM PARTON SCATTERING

As a starting point in this discussion we emphasize that the exclusive production channel $gg \rightarrow \bar{b}tH^-$ is a perturbatively well defined way to compute the total cross section as well as distributions for associated tH^- production. It is consistent in the sense that it includes the squared matrix element to order $\alpha_s^2 y_{b,t}^2$, where $y_{b,t}$ is the charged Higgs Yukawa coupling to the third generation quarks. Even though there might be some dispute concerning the precise numerical value of the bottom quark mass, the infrared divergences arising from the intermediate bottom quark propagators are regularized by this finite bottom quark mass. Once these bottom quarks are observed or even tagged, the bottom quark transverse momentum and rapidity become the relevant cutoff parameters to define the observable cross section including the detector acceptance cuts; they render the cross section after cuts almost independent of the actual value of the bottom mass, which would be the relevant cutoff parameter for the total cross section without acceptance cuts.

Beyond naive perturbation theory the integration over phase space of the final state bottom quark gives rise to possibly large logarithms [25]. As an illustration the typical gluon radiation off an incoming parton in Drell–Yan production processes leads to an asymptotic $1/p_{T,g}$ behavior in the gluon transverse momentum distribution. The same problem arises in exclusive charged Higgs boson production, where one of the two incoming gluons splits into two bottom quarks, eq.(1). Because the massive bottom propagator leads to an asymptotic transverse mass dependence $1/m_{T,b}$ instead of the transverse momentum $1/p_{T,b}$, the infrared divergence is regularized by the bottom mass. For small transverse bottom momenta the differential partonic cross section approaches the asymptotic form [26]

$$\begin{aligned} \frac{d\sigma^{(btH)}}{dp_{T,b}} &\sim \left. \frac{d\sigma^{(btH)}}{dp_{T,b}} \right|_{\text{asympt}} = S \frac{p_{T,b}}{m_{T,b}^2} = S \frac{p_{T,b}}{p_{T,b}^2 + m_b^2} \\ \sigma_{\text{tot}}^{(btH)} &\sim \left. \sigma_{\text{tot}}^{(btH)} \right|_{\text{asympt}} = \frac{S}{2} \log \left(\frac{\mu_F^2}{m_b^2} + 1 \right) \end{aligned} \quad (2)$$

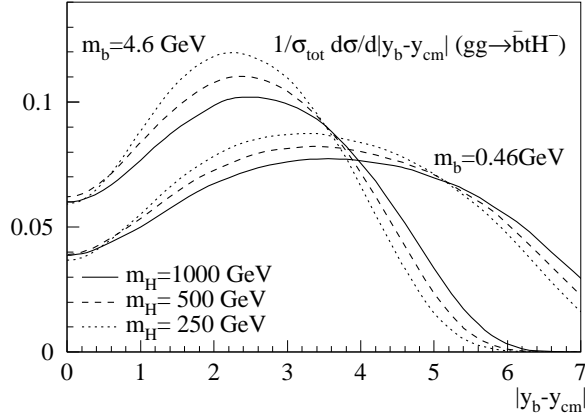


Figure 1. The rapidity difference between the final state bottom jet and the center of mass system for exclusive charged Higgs boson production at the LHC, eq.(1). The two sets of curves with three different charged Higgs boson masses are given for the physical on-shell bottom mass 4.6 GeV as well as for an arbitrarily chosen smaller bottom mass as the infrared regulator.

with a proportionality constant S , which we can link to the asymptotic total cross section. In contrast, for large transverse momentum $p_{T,b} \gg m_b$ we can safely neglect all bottom mass effects. The integration over the bottom phase space leads to logarithms $\log(p_{T,b}^{\max}/m_b)$. They are not divergent, but they can become quite large, though not as dramatically as for light quarks where Λ_{QCD} serves as the infrared cutoff. Switching to a bottom quark parton description ($bg \rightarrow tH^-$) corresponds to a resummation of these potentially large logarithms beyond naive perturbation theory. However, this procedure relies on several approximations, which should be carefully examined.

When describing the intermediate bottom as a parton we use the DGLAP evolution with the splitting kernels for massless particles. We assume that the bottom quark be massless.² In turn we also assume that at leading order the intermediate bottom quark and therefore the outgoing bottom jet are collinear with the incoming partons in the exclusive process. This approximation will never be perfect, since the cutoff parameter m_b is only slightly smaller than the minimum observable transverse momentum at a collider. But for the parton description of the bottom quark is it a necessary condition that the outgoing bottom in the exclusive cross section is clearly peaked forward. We show this behavior for exclusive charged Higgs boson production in Fig. 1. For the physical bottom mass the distribution is indeed peaked forward, and as expected the peak moves further out for smaller bottom masses. A detailed discussion of the error induced by the zero bottom mass approximation can be found in ref. [25,27].

After making sure that the collinear approximation describes the kinematics of the tree-level process $gg \rightarrow \bar{b}tH^-$ we still have to determine if there are large logarithms to resum. In the bottom parton approach

²This approximation does not have to include the bottom Yukawa coupling. We can consistently expand the cross section in terms of the bottom mass, extracting an over-all factor $y_{b,t}^2$ first. In other words, once we consider the Standard Model as an effective theory with massive fermions there is no link between the masses and the Yukawa couplings. This becomes obvious in the two Higgs doublet model, where we consistently neglect terms proportional to m_b , but keep terms proportional to $m_b(\tan\beta)^j$ ($j \geq 1$).

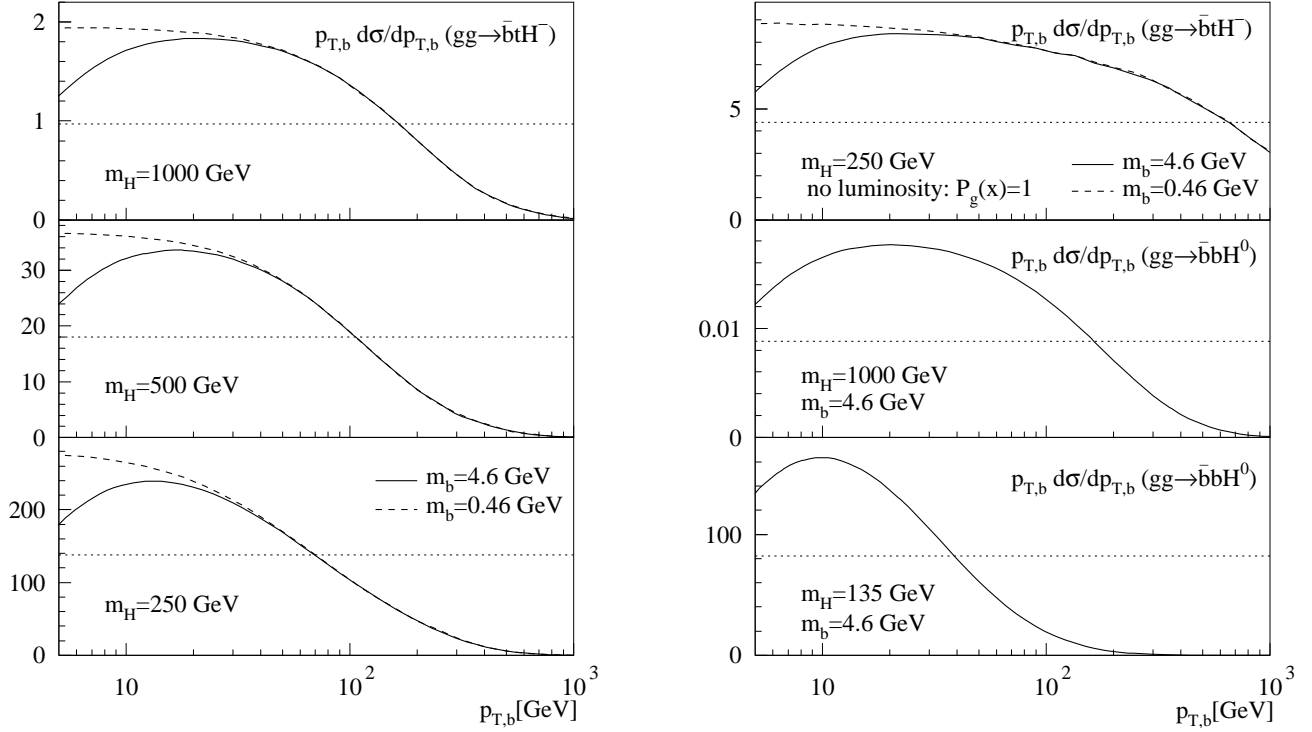


Figure 2. Left: the bottom transverse momentum distribution for exclusive charged Higgs boson production at the LHC, eq.(1). For all three Higgs masses the curves are given for the physical on-shell bottom mass 4.6 GeV as well as for an arbitrarily chosen smaller bottom mass as the infrared regulator. The thin dotted line indicates half the height of the plateau. The absolute normalization of the curves for the two infrared regulators is physical. Both curves coincide for large transverse momenta, where the bottom mass is negligible. Right: in the upper panel the same distribution for a heavy charged Higgs boson, but with the gluon luminosity set to unity $\mathcal{L}_{gg} \equiv 1$. Below this in the two lower panels the transverse momentum distribution for the bottom quarks in exclusive neutral Higgs boson production $gg \rightarrow \bar{b}bH$ for two neutral Higgs boson masses.

we approximate the complete differential cross section by an asymptotic $1/p_{T,b}$ or $1/m_{T,b}$ behavior. The upper boundary of the $p_{T,b}$ or $m_{T,b}$ integration defines the factorization scale μ_F of the bottom parton density and determines how big the resummed logarithms can be. After integrating out the final state bottom quark in the exclusive gluon fusion process the total hadronic cross section for $pp \rightarrow gb \rightarrow tH^-$ production becomes essentially proportional to $\log(\mu_F/m_b)$, as we would expect. While this $1/m_{T,b}$ behavior is by definition present even for large values of the transverse momentum in the matrix element for the corresponding Feynman diagram, this is not necessarily true for the differential hadronic cross section $d\sigma/dp_{T,b}$.

In Fig. 2 we show the $1/p_{T,b}$ behavior of the hadronic distributions for three different charged Higgs boson masses. All renormalization and factorization scales are set to the average final state particle mass. First of all we see how the zero bottom mass approximation breaks down when the transverse momentum is of the order of the bottom mass and a distinction between transverse mass and transverse momentum is necessary. Instead of a simple $1/p_{T,b}$ we indeed see the asymptotic form from eq.(2). If we replace the on-shell bottom mass with a smaller bottom mass the plateau extends to smaller transverse momentum, again confirming the asymptotic behavior. The small $p_{T,b}$ end of plateau in the transverse momentum spectrum, however, does not lead to large numerical effects, since the logarithm $\log(p_{T,b}^{\max}/m_b)$ and thereby the bottom

parton density vanish for a factorization scale $\mu_F = p_{T,b}^{\max} \sim m_b$.

Looking for large numerical effects we have to focus on the high $p_{T,b}$ end of the asymptotic regime. In the left panel of Fig. 2 we see how the high $p_{T,b}$ end of the plateau roughly scales with the average mass in the final state. This coincides neatly with the observation that the only scales allowed for the evaluation of total cross sections are external scales. They are typically chosen proportional to the average mass of the final state particles

$$\mu_F \sim C m_{\text{av}} = C \frac{m_t + m_H}{2} \quad (3)$$

where the proportionality factor C is arbitrary. The dependence on the choice of the scale and thereby on the choice of C vanishes after including all orders of perturbation theory. Comparing eq.(3) with Fig. 2 shows that the naive choice $C \sim 1$ is not obviously appropriate. Choosing $C \sim 1$ assumes large logarithms $\log(p_{T,b}^{\max}/m_b)$ being resummed to values $\mu_F \sim m_{\text{av}}$. This will yield an overestimate of the total cross section.

Using the asymptotic form of the cross section in eq.(2) we first note that the value of S should only very mildly depend on the numerical value of the bottom mass [25,26]. The same is true for the factorization scale, which only parameterizes the large transverse momentum regime. We can see from Fig. 2 that there the bottom mass effects are negligible. Evaluating the expression for the asymptotic total cross section for the two bottom masses we can determine the values of S and μ_F . As a check we compare the value of S , which is the predicted plateau value of $p_{T,b}d\sigma/dp_{T,b}$, with the plateau value we obtain from the complete calculation. We find them good agreement at least for a bottom mass of 0.46 GeV in the case where the plateau is not particularly well pronounced for the physics bottom mass. For the appropriate factorization scale we obtain 185, 120, 80 GeV for the three Higgs boson masses 1000, 500, 250 GeV. Very similar values we would naively obtain from Fig. 2, looking for the point where $p_{T,b}d\sigma/dp_{T,b}$ has dropped to half of the plateau value. This means that the appropriate factorization scale indeed scales with the average final state mass, eq.(3), but with $C \sim 1/3$. On the other hand we point out that for associated charged Higgs boson and top quark production we do always find a $p_{T,b}$ regime in which the hadronic differential cross section $d\sigma/dp_{T,b}$ shows the expected asymptotic behavior and therefore the bottom parton treatment is justified — but with an appropriate choice of the bottom parton factorization scale.

To understand where this unexpectedly narrow asymptotic plateau comes from we turn to the partonic cross section. In the right panel of Fig. 2 we show the transverse momentum distribution with the gluon luminosity set to unity ($\mathcal{L}_{gg} \equiv 1$). Still the interference between the different diagrams as well as the hadronic phase space limit the asymptotic behavior once we look at very large transverse momenta. If one would want to determine the bottom factorization scale for example from the $p_{T,b}$ value at which the plateau has dropped to half of its value, we find $\mu_F \sim 3m_{\text{av}}$ when we discard the gluon luminosity. The preferred low scales observed from the left panel of Fig. 2 are therefore entirely due to the steeply falling gluon density which suppresses any large transverse momentum radiation of forward bottom jets.

To prove the universality of our argument we show the same transverse bottom momentum distribution for the exclusive neutral Higgs boson production $gg \rightarrow b\bar{b}H$ [24] in the right panel of Fig. 2. This channel becomes important for large values of $\tan\beta$, where it supplements the inclusive Higgs production process via gluon fusion [2,8]. It can of course be evaluated as an exclusive process with incoming gluons $gg \rightarrow b\bar{b}H$. But it can also be regarded as partly [27] or completely inclusive, *i.e.* with one or two incoming bottom partons. The numerical effects of the resummation in the bottom parton approach can be as large as an order of magnitude for the total cross section. The same reasoning as for the charged Higgs boson

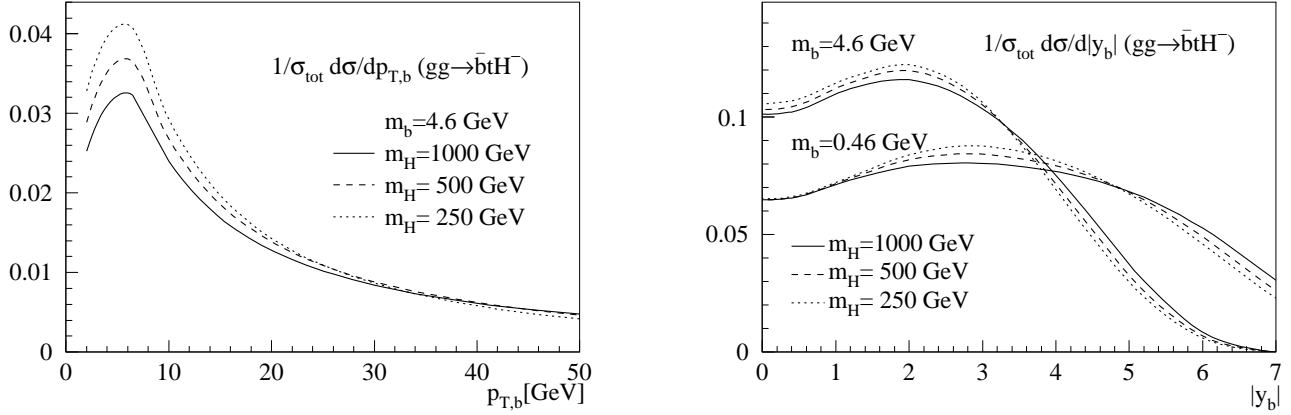


Figure 3. Left: the bottom transverse momentum distribution for exclusive charged Higgs production at the LHC, eq.(1). Right: the bottom rapidity distribution for the same process. Again a set of curves with a small infrared regulator is added ($m_b = 0.46$ GeV).

production applies in this case. First one shows that the bottom quarks are forward or for a small bottom mass collinear to the incoming gluons. Then one determines an appropriate choice of the factorization scale from the size of the asymptotic region in which the differential cross section shows the behavior as in eq.(2). One has to keep in mind that the expected asymptotic behavior (once it does not give a plateau in Fig. 2) shows non-negligible bottom mass effects. Therefore we emphasize that for differential cross sections at leading order the bottom parton approximation is not valid if the regime where the finite bottom mass ruins the $1/p_{T,b}$ behavior immediately blends into the regime where the gluon densities cut off the asymptotic behavior at large transverse momentum.

From the comparison of the two curves for a 1 TeV neutral and a 1 TeV charged Higgs boson we see that the behavior is very similar: the bottom parton description is valid, and the factorization scale should be chosen considerably below the average final state mass (for the charged Higgs boson) or below the Higgs mass (for the neutral Higgs boson). For a light neutral Higgs boson ($m_H = 135$ GeV) the asymptotic behavior only survives up to $p_{T,b} \lesssim 40$ GeV, in more detail depending on where one would like to draw the line. This corresponds to a logarithmic enhancement $\log(p_{T,b}/m_b) \lesssim \log 8 \sim 2$. Even more so for the Tevatron this leads to factorization scales where the bottom parton density decreases, and with it the enhancement of the total cross section, which is the effect of the resummation.³

Up to this point we have only talked about the validity of the bottom parton approximation and the correct choice of the factorization scale. However, the applicability of the bottom parton approach is very closely tied to the reason why the partly inclusive analyses are attractive: if the exclusive process exhibits a collinear final state bottom jet from gluon splitting this jet is not likely to hit the detector, much less to be tagged. For the exclusive $b\bar{t}H^-$ production we illustrate this feature in Fig. 3. Most of the bottom jets are not sufficiently central to be tagged and thereby significantly suppress the backgrounds. Moreover, the

³As we will show later, higher order QCD contributions to the inclusive processes [27] include the exclusive channel $gg \rightarrow b\bar{b}H$. For very small factorization scales this exclusive diagram becomes dominant and leads us back to the original exclusive cross section in a well defined manner, once we consider the next-to-leading order cross section.

bottom transverse momentum peaks around $p_{T,b} \sim m_b$, considerably too soft to be seen or even tagged with good efficiency. This means that the same feature which allows us to use the bottom parton approach makes it hard to utilize the exclusive process: the final state bottom jet is too collinear to be particularly useful.

Even though the exclusive cross section with the appropriate cuts — but without a required final state bottom jet — yields a well defined perturbative cross section prediction, the presence of collinear bottom jets can lead to large logarithms. They alter the convergence of the strictly perturbative power series. Therefore the inclusive process with the right choice of parameters gives a numerically improved cross section prediction. In the case in which the analysis does not require a final state bottom jet we strongly advocate use of the inclusive process, since the reliability of the cross section predictions will be significantly improved beyond naive perturbation theory.

III. NEXT-TO-LEADING ORDER RESULTS FOR A TWO HIGGS DOUBLET MODEL

To improve the theoretical cross section prediction and to reduce the theoretical uncertainty we compute the inclusive process $pp \rightarrow gb \rightarrow tH^-$ to next-to-leading order QCD. In this Section we present the results for a two Higgs doublet model. We would like to mention that part of the numbers presented in this section have been compared in detail with similar results given earlier in ref. [15]. For all diagrams included in both calculations the numbers agree within the uncertainties from different input parameters and from the scheme dependence in the top mass renormalization. The complete set of next-to-leading order QCD corrections include virtual gluon loops as well as real gluon radiation. The massive supersymmetric loops will be discussed in Section IV. The complete set of next-to-leading order processes consists of:

$$\begin{aligned}
gb &\rightarrow tH^- && \text{(Born term)} \\
gb &\rightarrow tH^- && \text{(virtual correction)} \\
gb &\rightarrow tH^-g \\
gg &\rightarrow tH^-\bar{b} \\
q\bar{q} &\rightarrow tH^-\bar{b} && b\bar{q} \rightarrow tH^-q && \bar{b}\bar{b} \rightarrow tH^-\bar{b} \\
bq &\rightarrow tH^-q && bb &\rightarrow tH^-b
\end{aligned} \tag{4}$$

The calculation is carried out in the dimensional regularization scheme. All ultraviolet poles are analytically cancelled between the virtual diagrams and the counter terms. The strong coupling and the bottom Yukawa coupling are renormalized in the $\overline{\text{MS}}$ scheme. This way α_s and $y_{b,t}$ both are running parameters, dependent on the same renormalization scale μ_R . As the renormalization scale we choose $\mu_R = m_{\text{av}}$. We expect logarithms from virtual corrections to be absorbed in the running mass definition, in complete analogy to Higgs decays to massive fermions [29]. The factorization and the renormalization scales are often identified for convenience, but there is no argument from first principles which enforces that choice. We will discuss this issue in detail below. The external top mass we renormalize in the on-shell scheme.

The infrared poles are also cancelled analytically between the virtual corrections, the real emission diagrams, and the mass factorization. The numerical impact of the higher order contributions is shown in Fig. 4. The leading order results are given for the running bottom mass as well as for the bottom pole mass in the Yukawa coupling. This choice is not fixed by first principles at leading order, whereas at next-to-leading order the counter term defines the bottom Yukawa coupling uniquely. The difference between these two mass definitions is strictly speaking part of the theoretical uncertainty for the leading order cross section

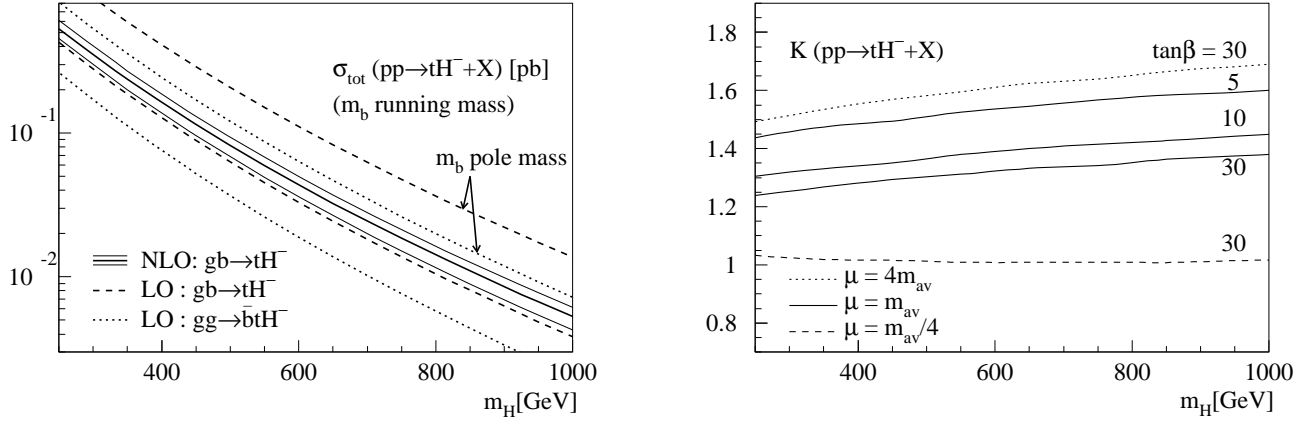


Figure 4. Left: the inclusive production cross section $pp \rightarrow tH^- + X$ at the LHC. The dashed and solid lines show the consistent leading order and next-to-leading order results. The dotted line is the total cross section from the exclusive production process, eq.(1). To illustrate the enhancement through large logarithms both tree level results are also quoted using the (inappropriate) pole mass for the bottom Yukawa coupling. The range for the next-to-leading order result is given for $\mu_F = \mu_R = m_{av}/4 \cdots 4m_{av}$. Right: the corresponding consistent K factors for the three values of $\tan\beta = 5, 10, 30$. In the case of $\tan\beta = 30$ we show three choices of $\mu = \mu_R = \mu_F$, consistently for leading order and next-to-leading order cross sections.

prediction. After adding all higher orders the cross section should be independent of the choice, as it should be independent of the renormalization and factorization scale. We want to stress, however, that it is well known that the pole mass Yukawa coupling always yields a huge overestimate of cross sections and decay widths and should generally not be used [29]. The band for the next-to-leading order cross section is given by a variation of the renormalization and factorization scale $\mu_R = \mu_F = (m_{av}/4, m_{av}, 4m_{av})$. From the discussion in Section II we know that for the factorization scale this is not a good choice. But we still fix the two scales for convenience at the central scale, which is preferred by the renormalization scale [29].

The size of the next-to-leading order corrections as a function of the charged Higgs boson mass and of the scale is shown in the right panel of Fig. 4. The K factor is defined consistently as $\sigma_{\text{NLO}}/\sigma_{\text{LO}}$, including the respective one or two loop running of the strong coupling and the third generation Yukawa couplings. The corrections seem to be perturbatively well under control, ranging from +30% to +40% for $\tan\beta = 30$ and Higgs boson masses between 250 and 1000 GeV. As expected the size of the K factor still depends on the choice of the scales.

In addition to the explicit K factor, the shift in the consistent bottom Yukawa coupling absorbs another factor $y_{b,2\text{-loop}}^2/y_{b,1\text{-loop}}^2 \sim 0.84$, while the top Yukawa coupling is more stable⁴, $y_{t,2\text{-loop}}^2/y_{t,1\text{-loop}}^2 \sim 1.0$. The next-to-leading order QCD corrections are flavor blind and proportional only to the Born coupling structure $y_{b,t}^2$, which as a function of $\tan\beta$ is either dominated by the top quark or by the bottom quark

⁴We could in principle use the 3-loop running bottom masses, which yields another factor $y_{b,3\text{-loop}}^2/y_{b,2\text{-loop}}^2 \sim 0.97$. The physical condition is again $m_b(m_b) = 4.2$ GeV. However, this way we would resum and absorb terms which are not explicitly included in the NLO cross section and the actual numerical improvement is not obvious and certainly not well under control.

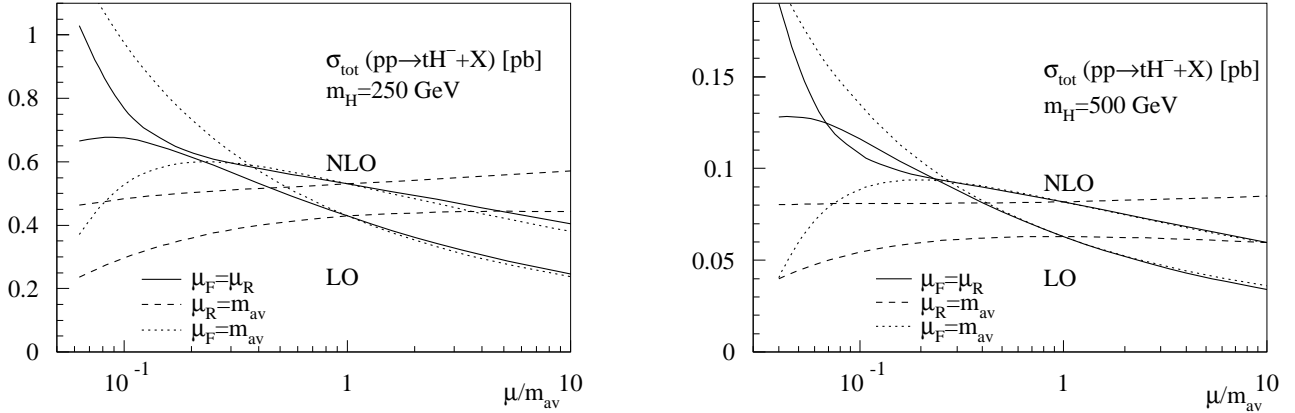


Figure 5. The variation of the total inclusive cross section $pp \rightarrow tH^- + X$ as a function of the renormalization and factorization scales, around the central value $\mu = m_{av}$, eq.(3). The two panels give the result for two different charged Higgs boson masses, 250 GeV and 500 GeV. The lower end of the curves corresponds to $\mu \sim 10$ GeV. The respective leading order and next-to-leading order curves can be identified at the point where they meet for the central choice $\mu = m_{av}$.

Yukawa coupling. In the right panel of Fig. 4 we show the K factor for three different values of $\tan \beta$ (the curve for $\tan \beta = 50$ is indistinguishable from $\tan \beta = 30$). The only difference between these three curves comes from the running Yukawa coupling: the running bottom Yukawa coupling, which is dominant for large values of $\tan \beta$, absorbs a larger correction than the running top Yukawa coupling. The consequence is a larger remaining K factor for smaller values of $\tan \beta$.

More detailed information concerning the scale variation is included in Fig. 5. As argued above, the appropriate choice for the factorization scale should scale with the average final state mass, but with a proportionality factor smaller than unity $\mu_F \sim 1/3 m_{av}$. In the discussion of the total cross section results we accommodate this effect by choosing a large window for the scale variation. From Fig. 5 we see that the dependence of the cross section on the factorization scale is mild. To leading order the dependence becomes large only once the bottom factorization scale comes close to the bottom mass. Since the bottom density comes from gluon splitting into two bottom quarks it has to be essentially proportional to $\log(\mu_F/m_b)$, *i.e.* it has to vanish for $\mu_F \rightarrow m_b$. This is precisely the behavior we see in the small scale regime for both Higgs boson masses. To next-to-leading order the scale dependence stays flat even for very small factorization scales. Assuming that the light flavor quark initiated processes listed in eq.(4) are suppressed at the LHC the purely gluon initiated process dominates for factorization scales $\mu_F \rightarrow m_b$. The large K factor is an artifact of the bottom parton approximation which leads to a vanishing leading order cross section, whereas the next-to-leading order saturates onto the light-flavor induced channels, which include the exclusive $gg \rightarrow \bar{b}tH^-$ process. This way the next-to-leading order inclusive calculation interpolates between the inclusive and the exclusive results⁵, where now the exclusive channel does not depend on the bottom mass as the infrared regulator. Instead all infrared poles cancel in the given order of perturbation

⁵It remains to be checked, however, how good this interpolation is numerically in the regime where the ‘large logarithms’ $\log(p_{T,b}/m_b)$ are only slightly enhanced.

theory. This means that at the one-loop level the inclusive cross section approaches the exclusive result in the limit of no large logarithms, where the enhancement through the resummation disappears. The only error left is the zero bottom mass approximation [28,27].

Once the charged Higgs boson is heavier than ~ 500 GeV the numerically dominant theoretical uncertainty comes from the unknown renormalization scale, dominantly from the scale of the strong coupling. While for a small factorization scale the total cross section decreases, a small renormalization scale yields a larger strong coupling and a larger running bottom mass. Identifying both scales inherently leads to a cancellation and therefore to a likely underestimate of the theoretical uncertainty. This can for example be taken care of by identifying a large renormalization scale with a small factorization scale [30].

On the other hand, the physics can easily be understood. For small factorization scales the cross section decreases slowly, until the factorization scale becomes close to the bottom mass, at which point it drops sharply. This reflects the logarithmic dependence of the bottom parton density. At next-to-leading order the drop is softened by the light-flavor induced channels, in particular with a purely gluonic initial state. At large scales the logarithmic dependence $\sim \log(\mu_F/m_b)$ is still present, but the variation has become very weak.

The renormalization scale dependence in contrast explodes for the leading order cross section at small scales long before reaching the bottom mass. At next-to-leading order it reaches a maximum, but the variation of the cross section is still considerably larger than the variation with the factorization scale. The cancellation between the renormalization and the factorization scale dependence has an interesting consequence, which we observe in Fig. 5. If we identify both scales and evaluate the cross section for very small values $\mu/m_{\text{av}} \lesssim 0.1$ the next-to-leading order prediction increases rapidly. Physically this is not a problem, since the scales have to be very small, which might be an appropriate choice for the factorization scale, but certainly not for the renormalization scale, as we argued above. We know that for these small scales the dependence on the logarithms $\log(\mu_F/m_b)$ and $\log(\mu_R/m_H)$ largely cancels. However, terms proportional to $\log(\mu_F/m_b) \times \log(\mu_R/m_H)$ in particular in the gg channel can become very large. One way to look at this effect is that the unphysically small renormalization scale gives a large negative prefactor for the factorization scale dependence, namely $\log(\mu_R^2/m_H^2)$. This dominates the factor in front of $\log(\mu_F/m_b)$, which for more appropriate renormalization scales is small and positive instead.

For a reasonably large renormalization scale almost the entire scale variation is driven by the renormalization scale; *i.e.* over almost the entire range the renormalization scale dominates the variation of the cross section with the scales. This effect is well known from supersymmetric particle production at the LHC. For processes mediated by a strong coupling at tree level, the scale variation is an appropriate measure for the theoretical uncertainty [22]. Again the change in the cross section is driven by the renormalization scale. On the other hand, for weakly interacting particles produced in Drell–Yan type processes, the leading order scale variation is dominated by the factorization scale and is not a good measure for the theoretical uncertainty [23]. For the inclusive associated charged Higgs boson and top quark production both, Fig. 4 and Fig. 5 show that the remaining theoretical uncertainty as derived from the renormalization and factorization scale dependence can be estimated to be $\lesssim 20\%$ for a central choice of scales.

To accommodate this behavior we stick to the identification of both scales $\mu_F = \mu_R = C m_{\text{av}}$, as defined in eq.(3). According to Fig. 5 this reflects the dominant scale variation of the cross section. In addition we follow our arguments of Section II and check that the cross section predictions are stable for small factorization scales, down to at least $\mu_F \sim m_{\text{av}}/3$. The graphs in Fig. 5 confirm that the cross sections

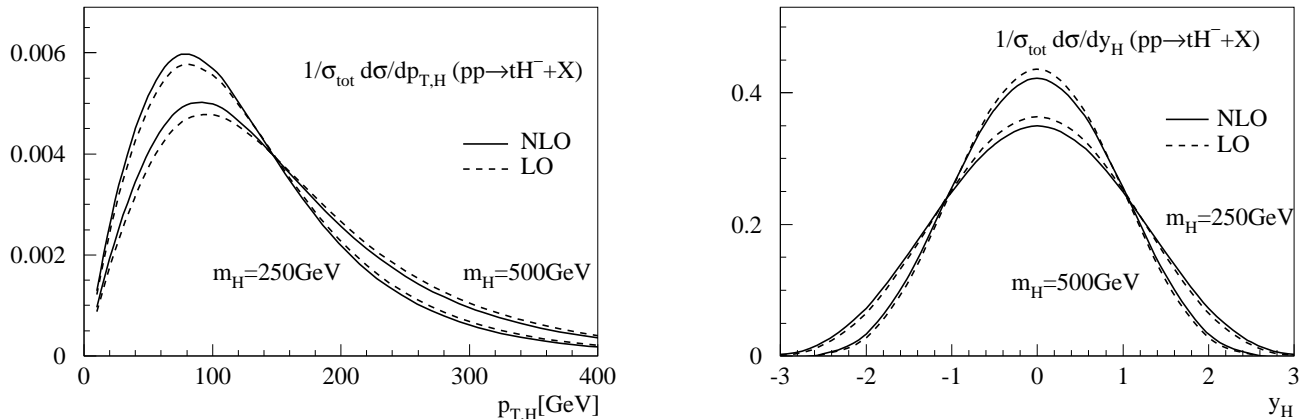


Figure 6. The charged Higgs boson transverse momentum and rapidity distributions for the inclusive process $pp \rightarrow tH^- + X$ are given for two different charged Higgs boson masses, 250 GeV and 500 GeV. The distributions are normalized to the total cross section and evaluated at the central scale $\mu = m_{av}$.

are stable down to factorization scales $\mu_F \lesssim m_{av}/10$, which also means that the inclusive charged Higgs boson production for $m_H \gtrsim m_t$ will not run into any problems with the bottom parton description.

Looking beyond the corrections to the total hadronic cross section we compute the transverse momentum and rapidity distributions for the charged Higgs boson. The normalized differential cross sections are depicted in Fig. 6. As expected, the impact of the higher order corrections on the shape of the rapidity distribution is small; the addition of the third final state particle does not alter the symmetric behavior around $y_H = 0$ at a pp collider. The effect on the charged Higgs boson transverse momentum is a systematic softening. One might have expected slightly harder charged Higgs bosons, with an additional gluon radiated off the top quark and both of them balanced by the Higgs boson. However, most of the jet radiation comes from the initial state. As seen in Section II, the radiation of high transverse momentum jets is cut off by the steeply falling partonic energy dependence of the gluon luminosities. This limited available energy directly translates into a softening of the Higgs boson transverse momentum, once a third final state particle is added to the process.

IV. NEXT-TO-LEADING ORDER RESULTS WITH SUPERSYMMETRY

Even though the Standard Model with a two doublet Higgs sector is a perfectly well-defined renormalizable theory, we are particularly interested in the MSSM version of this model. The MSSM fixes the parameters of the Higgs sector, links each of the Higgs doublets to up- or down-type fermions, normalizes the two gauge couplings to the Fermi coupling constant, and fixes all three- and four-scalar couplings. The number of free tree level parameters in the Higgs sector is reduced to two, which are usually chosen to be the pseudoscalar mass m_A and the ratio of the vacuum expectation values $\tan \beta$ [31].

At next-to-leading order, supersymmetric particles can propagate through loops and contribute to the cross section $bg \rightarrow tH^- + X$. Because supersymmetry is broken and all virtual particles are heavy these corrections are infrared finite. The ultraviolet poles have to be extracted and absorbed into supersymmetric contributions to the counter terms for bare Standard Model masses and coupling. All next-to-leading order

corrections to the total cross section coming from these supersymmetric loop diagrams we include in a supersymmetric correction factor

$$K_{\text{SUSY}} = \frac{\sigma_{\text{SUSY}} + \sigma_{\text{NLO}}}{\sigma_{\text{NLO}}} = 1 + \frac{1}{K} \frac{\sigma_{\text{SUSY}}}{\sigma_{\text{LO}}} \quad (5)$$

As in Section III we assume a massless bottom quark. In supersymmetry this adds a slight complication: the bottom squark mass matrix includes off-diagonal elements, which are parameterized as $-m_b(A_b + \mu \tan \beta)$. The splitting of the first term $m_b A_b$ into the bottom mass and a trilinear mass parameter is not enforced by the Lagrangean; in other words the combination $m_b A_b$ does not automatically have to vanish with a zero bottom quark mass. Similarly in the approximation of zero bottom mass m_b on the one hand and finite bottom Yukawa coupling $m_b \tan \beta$ on the other, this off-diagonal matrix element will not vanish either. The off-diagonal term induces a mixing between the supersymmetric partner of the left and right handed bottom quark: we have to work with mass eigenstates $\tilde{b}_{1,2}$ instead of interaction eigenstates $\tilde{b}_{L,R}$ even in the limit of a vanishing bottom mass.

At one-loop order this off-diagonal entry can connect a left handed with a right handed bottom quark. Even though in the final result we neglect the bottom mass we do have to take into account this contribution to the bottom mass counter term. Mass counter terms have to be proportional to the bare mass $\delta m_b \propto m_b$; in this special case we find that in the on-shell mass renormalization scheme $\delta m_b \propto \sin(2\theta_b)$, with an implicit dependence $\sin(2\theta_b) \propto m_b(A_b + \mu \tan \beta)$. This gives back the proportionality to the bare mass, but as argued above it means that the contribution to the mass counter term has to be kept even in the zero bottom mass approximation. As shown in a series of papers this mass counter terms modifies the relation between the bottom mass and the bottom Yukawa coupling [33,34]:

$$\begin{aligned} \frac{m_b \tan \beta}{v} &\rightarrow \frac{m_b \tan \beta}{v} \frac{1}{1 + \Delta m_b} \\ \Delta m_b &= \frac{\sin(2\theta_b)}{m_b} \frac{\alpha_s}{4\pi} C_F m_{\tilde{g}} \frac{1}{i\pi^2} \left[B(0, m_{\tilde{b},2}, m_{\tilde{g}}) - B(0, m_{\tilde{b},1}, m_{\tilde{g}}) \right] \\ &= \frac{\alpha_s}{4\pi} C_F m_{\tilde{g}} (A_b + \mu \tan \beta) I(m_{\tilde{b},1}, m_{\tilde{b},2}, m_{\tilde{g}}) \\ I(a, b, c) &= -\frac{1}{(a^2 - b^2)(b^2 - c^2)(c^2 - a^2)} \left[a^2 b^2 \log \frac{a^2}{b^2} + b^2 c^2 \log \frac{b^2}{c^2} + c^2 a^2 \log \frac{c^2}{a^2} \right] \end{aligned} \quad (6)$$

The functions $B(0, m_{\tilde{b}}, m_{\tilde{g}})$ are the usual scalar two-point functions with the integration measure $d^n q$, $C_F = 4/3$ is the color factor. From eq.(6) we immediately see that the Δm_b correction is a finite mass renormalization of the external bottom legs. The correction as written in eq.(6) is already resummed over the string of external one-loop wave function corrections. The authors of ref. [34] have shown that this correction is the leading term in powers of $\tan \beta$. The reason why this contribution is usually referred to as non-decoupling is that for large supersymmetric particle masses in the loop *and for a large trilinear mass parameter A_b or higgsino mass parameter μ* , the correction to the Yukawa coupling does not vanish. This is well understood, since at the one-loop level it couples the ‘wrong’ Higgs doublet to the bottom quarks. The large one-loop correction does therefore not mean that perturbation theory breaks down. At the two-loop level the corrections should be small again. The Δm_b factor is not the only non-decoupling contribution in the MSSM either, as we would expect from the three scalar vertex $\tilde{b}_2 \tilde{t}_1 H^-$, which is again proportional

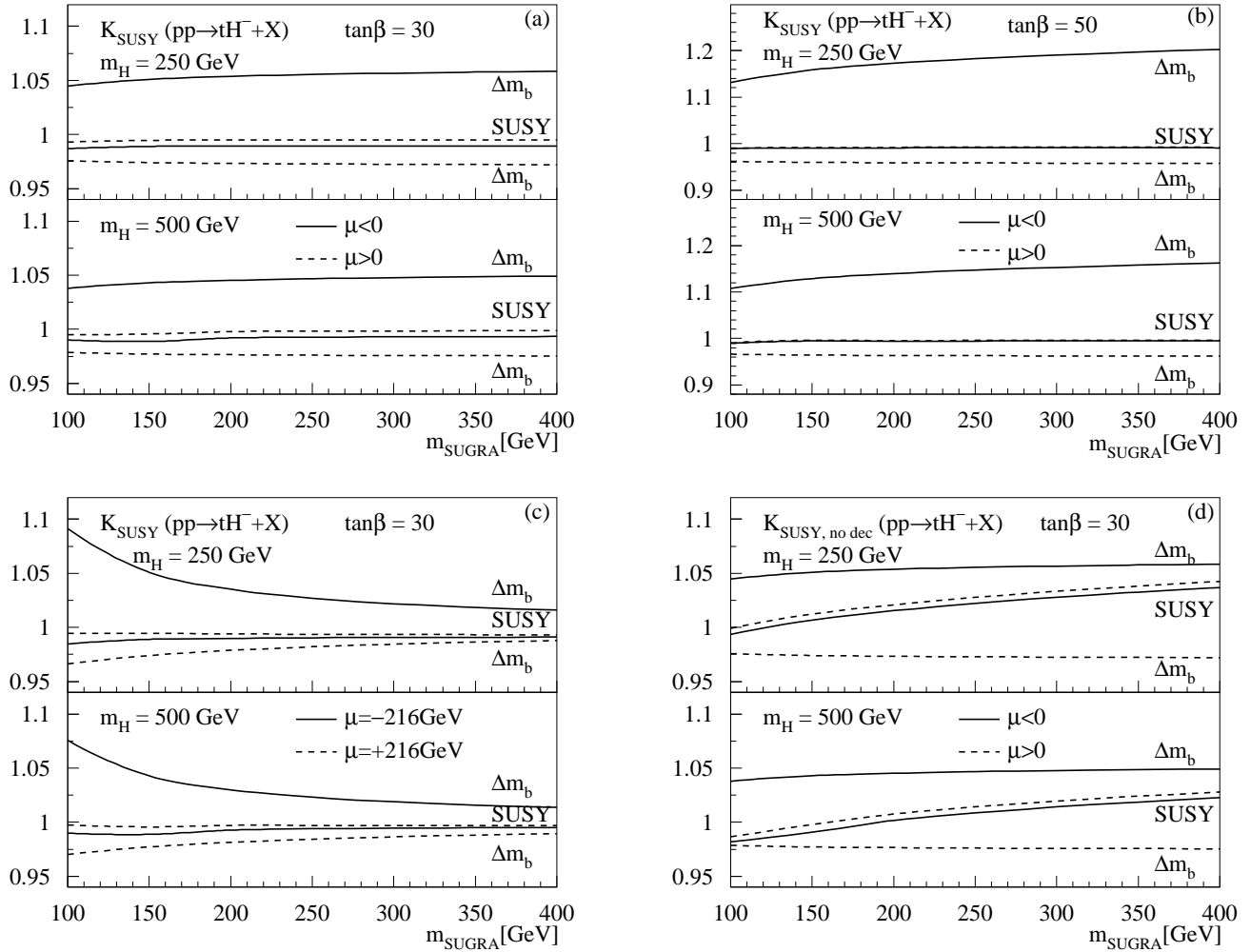


Figure 7. The dependence of the total cross section $pp \rightarrow tH^- + X$ on supersymmetric loop contributions. The enhancement factor is defined in eq.(5). The curves with the typically larger deviation from the two Higgs double model include Δm_b corrections only, the curves labeled SUSY include the complete remaining set of loop supersymmetric diagrams. All curves are given for two different Higgs boson masses (upper/lower panel) and for two signs of μ (solid/dashed line). The mass scale is defined as $m_{\text{SUGRA}} = m_0 \equiv m_{1/2}$: (a) corrections for $\tan \beta = 30$ and with a running higgsino mass parameter μ ; (b) same as (a), but with $\tan \beta = 50$; (c) same as (a), but with μ fixed at its value for $m_{\text{SUGRA}} = 150$ GeV; (d) same as (a), but without decoupling the heavy spectrum from the running Yukawa coupling. The range of particle masses covered by $m_{\text{SUGRA}} = 100 \dots 400$ GeV are for the gluino mass 284...1017 GeV, for the sbottom masses 212...827 GeV and 265...901 GeV, and for the stop masses 199...687 GeV and 326...895 GeV. The higgsino mass parameter runs from $|\mu| = 136 \dots 595$ GeV, except for in part (c).

to $m_b(\mu - A_b \tan \beta)$ [32]. But the Δm_b corrections for large values of $\tan \beta$ and small values of A_b are expected to be dominant. This regime is precisely where the charged Higgs boson search is promising.

To estimate how good the leading $\tan \beta$ approximation given by Δm_b is, we also compute the whole set of MSSM loop diagrams. The result for two different Higgs boson masses is shown in Fig. 7(a). None of the supersymmetric corrections show a considerable dependence on the supersymmetric mass scale. To simplify

the presentation we choose a diagonal line in the mSUGRA parameter space [35]: the scalar and gaugino mass scales are identified $m_{\text{SUGRA}} = m_0 \equiv m_{1/2}$ ⁶. The values for $\tan\beta = 30$ and $A_0 = 0$ are fixed, giving $A_b = 0$ at the electroweak scale. For the Δm_b corrections the sign of the higgsino mass parameter is crucial: for $\mu < 0$ we find $\Delta m_b < 0$, which according to eq.(6) enhances the cross section. For the opposite sign of μ the Δm_b corrections to the production cross section are negative. The supersymmetric corrections apart from the Δm_b corrections are negligible in comparison with the Δm_b terms. This is a feature of the large value of $\tan\beta$ and is even more pronounced for $\tan\beta = 50$ in Fig. 7(b). We note, however, that the picture changes significantly once we do not run the higgsino mass parameter $|\mu|$ to large values, together with the other heavy supersymmetric masses. In that case the Δm_b corrections decouple as shown in Fig. 7(c). Moreover, for a value $\tan\beta = 10$ the Δm_b correction drops below a $\pm 2\%$ effect, becoming even smaller than the explicit MSSM loop corrections. We note, however, that choosing large values for $\tan\beta$ and $|\mu|$ can in principle lead to almost arbitrarily large Δm_b effects, only limited by unitarity constraints.

Heavy particle loops contribute to both the running strong coupling $\alpha_s(\mu_R)$ and the third generation Yukawa coupling $y_{b,t}(\mu_R)$. They give rise to supersymmetric counter terms and thereby yield a logarithmic divergence $\log(m_{\text{heavy}}/\mu_R)$ in the cross section. On the other hand we use Standard Model measurements for these observables, which means that their running has to be governed by the light particle beta function [22,23]. The contributions from heavy particles to their beta function has to be explicitly cancelled, and as expected this decoupling absorbs all logarithmically divergences in the one-loop cross section. We show the (misleading) result one would get without decoupling the heavy particles from the running Yukawa coupling in Fig. 7(d)⁷.

V. SUMMARY

We have computed the complete next-to-leading order contributions to the inclusive cross section $pp \rightarrow tH^-$ in a general two Higgs double model and in the MSSM. We show why the bottom parton approach is valid for this process and gives a numerically reliable prediction for the cross section.

The one-loop contributions hugely improve the theoretical uncertainty of the leading order cross section prediction, in which one formally would still have the choice of using a pole mass or a running mass bottom Yukawa coupling. At next-to-leading order we fix the counter term to the running Yukawa coupling and check the cross section dependence on the renormalization and the factorization scale. Both lead to an uncertainty of $\lesssim 20\%$ on the total cross section. The impact on rapidity and transverse momentum distributions is tested and well under control. The over-all corrections to the total cross section in the two Higgs double model range between $+30\%$ and $+40\%$ for Higgs boson masses between 250 and 1000 GeV for the average final state mass scale choice.

⁶The next-to-leading order calculation is done with a completely general MSSM spectrum. The Fortran90 code can be obtained from tilman.plehn@cern.ch.

⁷We note that the decoupling in all curves of Fig. 7(a)-(c) is computed assuming that all heavy supersymmetric particle masses, the gluino mass, the two sbottom masses and the two stop masses, are degenerate. This leads to the simple decoupling term $m_{b,t}(\mu_R) \rightarrow m_{b,t}(\mu_R)[1 + \alpha_s/(4\pi)C_F \log(\mu_R^2/m_{\text{heavy}}^2)]$. The decoupling term for the strong coupling constant is as usually split into contributions from each heavy particle, including the top quark [22,23].

In case of a charged Higgs boson in the MSSM two kinds of supersymmetric corrections appear in addition: the on-shell renormalization of the bottom quark mass alters the relation between the bottom mass and the bottom Yukawa coupling. These Δm_b corrections are the leading supersymmetric one-loop corrections with respect to powers of $\tan \beta$. Their effect on the total cross section in a simple mSUGRA model we estimate to stay below $\pm 5\%$ for $\tan \beta = 30$ and below $\pm 20\%$ for $\tan \beta = 50$. Because the charged Higgs boson searches are most promising in the large $\tan \beta$ regime the remaining explicit supersymmetric loop diagrams only contribute on a negligible few percent level.

ACKNOWLEDGMENTS

I would like to thank Dieter Zeppenfeld for numerous enlightening discussions without which this paper could not have been written. Michael Spira I would like to thank for carefully reading the manuscript and being of great help through various interesting discussions. Tao Han, Ed Berger, and in particular Jing Jiang I would like to thank for discussions during an early stage of this project. I would like to thank Elzbieta Richter-Was and Dave Rainwater for their curiosity and their encouragement to publish these results. Dave Rainwater and Dieter Zeppenfeld I also want to thank for carefully reading the manuscript. Last but not least I would like to thank Shouhua Zhu for the efficient and pleasant comparison of his results [15] with the ones presented in this paper.

This research was supported in part by the University of Wisconsin Research Committee with funds granted by the Wisconsin Alumni Research Foundation and in part by the U. S. Department of Energy under Contract No. DE-FG02-95ER40896.

Bibliography

- [1] D. Abbaneo *et al.* [ALEPH Collaboration], arXiv:hep-ex/0112021.
- [2] Z. Kunszt and F. Zwirner, Nucl. Phys. B **385**, 3 (1992); ATLAS TDR, report CERN/LHCC/99-15 (1999); CMS TP, report CERN/LHCC/94-38 (1994); M. Spira, Fortsch. Phys. **46**, 203 (1998); D. Zeppenfeld, R. Kinnunen, A. Nikitenko and E. Richter-Was, Phys. Rev. D **62**, 013009 (2000); N. Kauer, T. Plehn, D. Rainwater and D. Zeppenfeld, Phys. Lett. B **503**, 113 (2001). V. Drollinger, T. Müller and D. Denegri, report CMS-NOTE-2002-006, arXiv:hep-ph/0201249.
- [3] D. Rainwater, D. Zeppenfeld and K. Hagiwara, Phys. Rev. D **59**, 014037 (1999); T. Plehn, D. Rainwater and D. Zeppenfeld, Phys. Lett. B **454**, 297 (1999) and Phys. Rev. D **61**, 093005 (2000).
- [4] W. Beenakker, S. Dittmaier, M. Krämer, B. Plümper, M. Spira and P. M. Zerwas, Phys. Rev. Lett. **87**, 201805 (2001); L. Reina, S. Dawson and D. Wackerroth, Phys. Rev. D **65**, 053017 (2002); F. Maltoni, D. Rainwater and S. Willenbrock, arXiv:hep-ph/0202205; A. Belyaev and L. Reina, arXiv:hep-ph/0205270.
- [5] T. Plehn, D. Rainwater and D. Zeppenfeld, Phys. Rev. Lett. **88**, 051801 (2002).
- [6] O. J. Éboli and D. Zeppenfeld, Phys. Lett. B **495**, 147 (2000).
- [7] E. Accomando *et al.* [ECFA/DESY LC Physics Working Group Collaboration], Phys. Rept. **299**, 1 (1998); J. A. Aguilar-Saavedra *et al.* [ECFA/DESY LC Physics Working Group Collaboration], TESLA TDR, report DESY-2001-011C.
- [8] R. K. Ellis, I. Hinchliffe, M. Soldate and J. J. van der Bij, Nucl. Phys. B **297**, 221 (1988); C. Kao and N. Stepanov, Phys. Rev. D **52**, 5025 (1995); for Standard Model searches see also: T. Plehn and D. Rainwater, Phys. Lett. B **520**, 108 (2001); T. Han and B. McElrath, Phys. Lett. B **528**, 81 (2002).
- [9] E. Eichten, I. Hinchliffe, K. D. Lane and C. Quigg, Rev. Mod. Phys. **56**, 579 (1984) [Addendum-ibid. **58**, 1065 (1986)]; N. G. Deshpande, X. Tata and D. A. Dicus, Phys. Rev. D **29**, 1527 (1984).
- [10] J. F. Gunion, H. E. Haber, F. E. Paige, W. K. Tung and S. S. Willenbrock, Nucl. Phys. B **294**, 621 (1987); D. A. Dicus, J. L. Hewett, C. Kao and T. G. Rizzo, Phys. Rev. D **40**, 787 (1989). W. Hollik and S. H. Zhu, Phys. Rev. D **65**, 075015 (2002).
- [11] S. S. Willenbrock, Phys. Rev. D **35**, 173 (1987); A. Krause, T. Plehn, M. Spira and P. M. Zerwas, Nucl. Phys. B **519**, 85 (1998); S. H. Zhu, C. S. Li and C. S. Gao, Phys. Rev. D **58**, 055007 (1998); O. Brein and W. Hollik, Eur. Phys. J. C **13**, 175 (2000); O. Brein, W. Hollik and S. Kanemura, Phys. Rev. D **63**, 095001 (2001).
- [12] D. A. Dicus and C. Kao, Phys. Rev. D **41**, 832 (1990); A. A. Barrientos Bendezu and B. A. Kniehl, Phys. Rev. D **59**, 015009 (1999); and Phys. Rev. D **63**, 015009 (2001); S. Moretti and K. Odagiri, Phys. Rev. D **59**, 055008 (1999).
- [13] A. C. Bawa, C. S. Kim and A. D. Martin, Z. Phys. C **47**, 75 (1990); F. Borzumati, J. L. Kneur and N. Polonsky, Phys. Rev. D **60**, 115011 (1999); A. Belyaev, D. Garcia, J. Guasch and J. Sola, arXiv:hep-ph/0203031.
- [14] L. G. Jin, C. S. Li, R. J. Oakes and S. H. Zhu, Eur. Phys. J. C **14**, 91 (2000).
- [15] S. H. Zhu, arXiv:hep-ph/0112109.
- [16] M. Drees and D. P. Roy, Phys. Lett. B **269**, 155 (1991); D. P. Roy, Phys. Lett. B **283**, 403 (1992); J. F. Gunion, Phys. Lett. B **322**, 125 (1994); V. D. Barger, R. J. Phillips and D. P. Roy, Phys. Lett. B **324**, 236 (1994); K. Odagiri, Phys. Lett. B **452**, 327 (1999); S. Moretti and D. P. Roy, Phys. Lett. B **470**, 209 (1999).
- [17] D. P. Roy, Phys. Lett. B **277**, 183 (1992); and Phys. Lett. B **459**, 607 (1999).

- [18] K. A. Assamagan and Y. Coadou, *Acta Phys. Polon. B* **33**, 707 (2002); K. A. Assamagan, Y. Coadou and A. Deandrea, report ATL-COM-PHYS-2002-002, arXiv:hep-ph/0203121.
- [19] D. Denegri *et al.*, report CMS-NOTE-2001-032, arXiv:hep-ph/0112045.
- [20] H. L. Lai *et al.* [CTEQ Collaboration], *Eur. Phys. J. C* **12**, 375 (2000).
- [21] S. Narison, *Phys. Lett. B* **341**, 73 (1994); we use the numerical implementation in: A. Djouadi, J. Kalinowski and M. Spira, *Comput. Phys. Commun.* **108**, 56 (1998).
- [22] W. Beenakker, R. Höpker, M. Spira and P. M. Zerwas, *Nucl. Phys. B* **492**, 51 (1997); W. Beenakker, M. Krämer, T. Plehn, M. Spira and P. M. Zerwas, *Nucl. Phys. B* **515**, 3 (1998).
- [23] W. Beenakker, M. Klasen, M. Krämer, T. Plehn, M. Spira and P. M. Zerwas, *Phys. Rev. Lett.* **83**, 3780 (1999).
- [24] J. Dai, J. F. Gunion and R. Vega, *Phys. Lett. B* **345**, 29 (1995); D. Froidevaux and E. Richter-Was, *Z. Phys. C* **67**, 213 (1995); D. Rainwater, M. Spira and D. Zeppenfeld, proc. Les Houches, 2001, arXiv:hep-ph/0203187.
- [25] J. C. Collins and W. K. Tung, *Nucl. Phys. B* **278**, 934 (1986); M. A. Aivazis, J. C. Collins, F. I. Olness and W. K. Tung, energies,” *Phys. Rev. D* **50**, 3102 (1994); F. I. Olness and W. K. Tung, *Nucl. Phys. B* **308**, 813 (1988); R. M. Barnett, H. E. Haber and D. E. Soper, *Nucl. Phys. B* **306**, 697 (1988); J. C. Collins, *Phys. Rev. D* **58**, 094002 (1998).
- [26] see *e.g.* M. Spira, plenary talk, SUSY2002, DESY.
- [27] C. S. Huang and S. H. Zhu, *Phys. Rev. D* **60**, 075012 (1999); J. Campbell, R. K. Ellis, F. Maltoni and S. Willenbrock, arXiv:hep-ph/0204093.
- [28] D. A. Dicus and S. Willenbrock, *Phys. Rev. D* **39**, 751 (1989); D. Dicus, T. Stelzer, Z. Sullivan and S. Willenbrock, *Phys. Rev. D* **59**, 094016 (1999).
- [29] E. Braaten and J. P. Leveille, *Phys. Rev. D* **22**, 715 (1980). S. G. Gorishnii, A. L. Kataev and S. A. Larin, *Sov. J. Nucl. Phys.* **40**, 329 (1984) [*Yad. Fiz.* **40**, 517 (1984)]; A. L. Kataev and V. T. Kim, *Mod. Phys. Lett. A* **9**, 1309 (1994); K. Melnikov, *Phys. Rev. D* **53**, 5020 (1996).
- [30] R. V. Harlander and W. B. Kilgore, arXiv:hep-ph/0201206.
- [31] J. F. Gunion, H. E. Haber, G. L. Kane and S. Dawson, “The Higgs Hunter’s Guide”, SCIPP-89/13; and arXiv:hep-ph/9302272.
- [32] L. G. Jin, C. S. Li, R. J. Oakes and S. H. Zhu, *Eur. Phys. J. C* **14**, 91 (2000); L. G. Jin, C. S. Li, R. J. Oakes and S. H. Zhu, *Phys. Rev. D* **62**, 053008 (2000); G. P. Gao, G. R. Lu, Z. H. Xiong and J. M. Yang, arXiv:hep-ph/0202016.
- [33] L. J. Hall, R. Rattazzi and U. Sarid, *Phys. Rev. D* **50**, 7048 (1994); M. Carena, M. Olechowski, S. Pokorski and C. E. Wagner, *Nucl. Phys. B* **426**, 269 (1994); A. Belyaev, D. Garcia, J. Guasch and J. Sola, *Phys. Rev. D* **65**, 031701 (2002).
- [34] M. Carena, D. Garcia, U. Nierste and C. E. Wagner, *Nucl. Phys. B* **577**, 88 (2000).
- [35] M. Drees and S. P. Martin, report MAD-PH-95-879, arXiv:hep-ph/9504324.